Chapter 14
Microstructure of the Nanostructured Oxide Composite Thin Films and Its Functional Properties

Xingkun Ning

14.1 Introduction

Nanocomposite oxide film is one of the most important research topics in nanoscale devices and sensors since availability of appropriate nanomaterial represents the foundation for exploring novel physical properties and applications associated with the nanometer length scale. The coexistence of multi-physical properties of the two phases engenders the material with the "product" property (i.e., the composite exhibits responses that are not available in the individual component phases), thus allowing an additional degree of freedom in the design of actuators, transducers, and storage devices [1]. For example, nanocomposite films of FE material with a FM have been synthesized toward future devices based on the control of magnetization with an electric field [2, 3], nanocomposite films of binary oxide with the manganites are particularly interesting as designing the memory-readers of digital devices and magnetic sensor due to the large values of low field magnetoresistance (LFMR) effect [4–6], and nanocomposite films combined of nanoparticles of noble metal and the CD oxides or DE oxides could potentially be applied for the electrode or optical devices as the enhanced conductivity or optical properties [7–10]. In addition, the phases with various well-controlled sizes and morphologies in the self-assembled nanocomposite films have attracted tremendous attention for creating a range of nanoscale structure types, leading to novel functionalities by interface coupling between the constituents [5, 11].

In this chapter, a basic characterization of the microstructure of the self-assembled nanocomposite oxide films is given together with general description of the forming mechanism. Then the typical microstructure and the corresponding

X. Ning (✉)
Hebei Key Lab of Optic-electronic Information and Materials, The College of Physics Science and Technology, Hebei University, Baoding 071002, People's Republic of China
e-mail: xkning@alum.imr.ac.cn

T. Li, Z. Liu (eds.), *Outlook and Challenges of Nano Devices, Sensors, and MEMS*,
DOI 10.1007/978-3-319-50824-5_14

physical properties in some simple oxide nanocomposite, multiferroics based, manganites based, and CD or DE based nanocomposite films, are described, followed by some discussions on the potential applications. In this chapter we confine ourselves to phenomenological descriptions where the microstructure and the interface coupling are mainly taken into account with simple structure models and circuit models.

14.2 Growth Mechanisms

Research in oxide nanocomposites-artificially created various microstructures involving transition metal oxide compounds-has flourished over the last decade [12, 13]. With the developments during the past decade in our ability to make extremely high quality nanocomposite oxide films, and therefore the corresponding microstructure, considerable interest has now grown in the science of microstructure-related and microstructure-tuned functionalities [14, 15]. It is then noted that designing the microstructure of the nanocomposite films is most important to tune the physical properties. In order to be able to modulate the microstructures, one of the key issues of research focus in this context is the mechanism of nanocomposite film growth and the corresponding microstructure.

14.2.1 Nucleation and Growth

For the nanocomposite oxide films with nucleation and growth mechanism, the themodynamics of the two phase, ratios of the two phase, epitaxial growth relation with the substrates (Fig. 14.1) and the surface/interface energies play important role in determining the microstructure of the nanocomposite films. On the one hand, there is no doubt that the volume ratio of the two phases plays critical role in determining the mircostructure. In general, when the ratios are much larger than 1:1, nanogranular microstructure would formed with the majority phase as the parent phase and the minority phase as the second phase. For the system with nearly equally content, the form of the microstructure depend on the different surface and interficial energies of the two phase. Under these circumstance, the microstructure of the nanocomposite films could be modulated by different substrate or using different crystal orientations. For example, as shown in Fig. 14.1, in a model $BiFeO_3/CoFe_2O_4$ (BFO/CFO)system, a (001) substrate results in rectangular-shaped CFO nanopillars in a BFO matrix; in contrast, a (111) substrate leads to triangular-shaped BFO nanopillars in a CFO matrix, dependent on the surface and interface energy [16]. On the other hand, he thermodynamics of the two phases strongly affect the microstructure of the nanocomposite films. With lower growth rate and higher insitu deposition temperature, the second phase completely wets the parent phase, forming the nanocolumnar structure embed in the parent

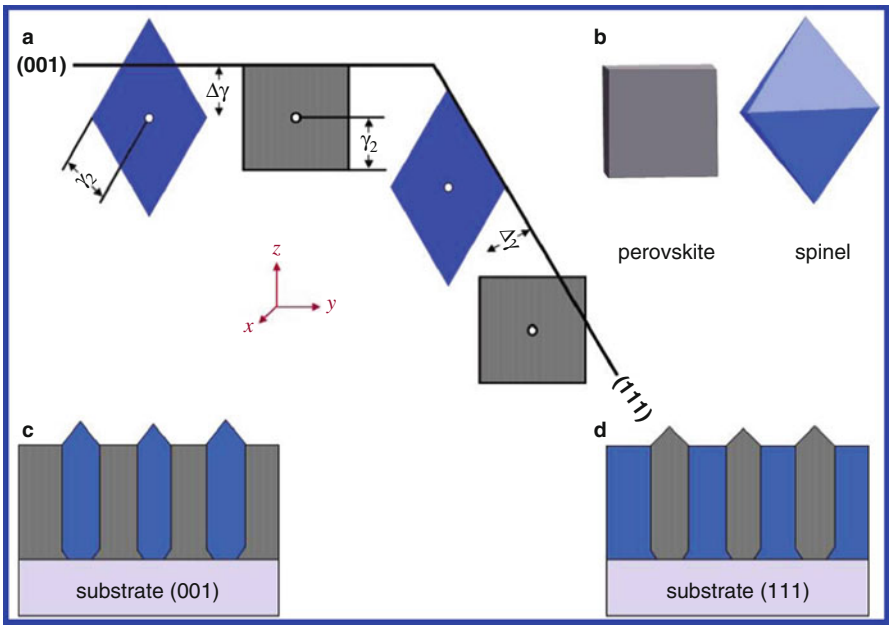

Fig. 14.1 Schematics of perovskite-spinel nanostructures on the (100) and (111) surfaces of $SrTiO_3$[16]

phase. In contrast, with higher growth rate and lower in-situ deposition temperature, the random nanoparticles structure forms instead of nanocolumnar structure because the insufficient kinetic energy to nucleate and grow on the surface of the parent phase, forming the nanogranular structure.

14.2.2 Spinodal Decomposition

Spinodal decomposition is a mechanism for the rapid unmixing of a mixture of liquids or solids from one thermodynamic phase, to form two coexisting phases. Spinodal decomposition can be constrasted with nucleation and growth where it occurs when the mixture is such that there is essentially no barrier to nucleation of the new phase. Recently, spinodal decomposition is of interest for the oxide materials which are mainly depend on the temperature, oxygen vacancy and distortion [17]. As have been reported in the $BaTiO_3$ (BTO)/STO self-assembled nanocomposite films, it is only possible that the spinodal decomposition happen around 300°C [18]. The microstructure after the spinodal decomposition is determined by the oxygen content and the distortion. Research in distortion-induced spinodal decomposition at the nanocomposite has recently. For example, the ordered nanocheckerboard-like structure have been reported in

the $Mg(Mn,Fe)_2O_4$ spinel structure [19]. In addition to this, Guion et al. also have been found the nanocheckerboard-like structure in the $(Nd_{1-x}Li_x)TiO_3$ perovskite structure [20]. In the year of 2008, Park et al. have found this structure in the $ZnMnGaO_4$ films at the first time, and then after spinodal decomposition is one of the main tools to modulated the microstructure and the corresponding physical properties [21].

14.2.3 Pseudo-Spinodal Decomposition

Pseudo-spinodal growth contains of both spinodal decomposition and nucleation and growth and was first observed in metallic alloy systems more than 20 years ago [22]. Although this phase transition is in line with the spinodal decomposition, the interfacial energy and the lattice distortion energy should be taken into account when using the Gibbs free energy to describe the nucleation and growth [23]. Thus, compared the spinodal decomposition, the pseudo-spinodal decomposition can be modulated by various. In 2009, Ni et al. showed that the nanocheckerboard oxide films are formed by pseudo-spinodal decomposition instead of spinodal decomposition through computer simulation. Since then, the growth mechanism of pseudo-spinodal decomposition becomes an important research area in nanocomposite films [24].

14.3 Synthesis and Microstructure

In the nanocomposite films, microstructures with nanogranular, nanomultilayer, nanocolumnar and nanocheckerboard characteristics can be divided according to the size, shape, distribution, arrangement and other characteristics of the second phase. Figure 14.2 shows the cross-sectional schematic view of the structure of nanogranular, nanomultilayer, nanocolumnar. Nanogranular (0-3 structure) configuration means that there are two phases in the composite, one consisting of zero-dimension particulates with the same shape and size, and the other is three-dimensional bulk [25]. Nanomultilayer (2-2 structure) refers to that the second phase and the parent phase are layered with each other. At last, the nanocolumnar (1-3 structure) refers to that the second phase formed columnar structure which uniformly embedded in the parent phase.

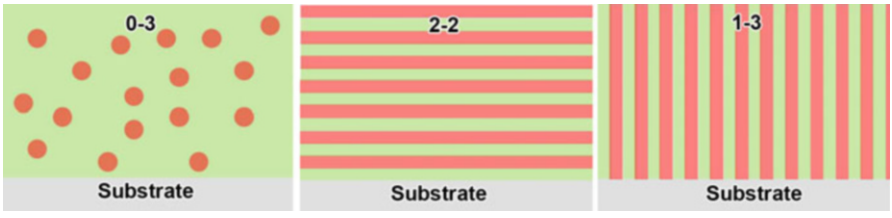

Fig. 14.2 Schematic of the 0-3, 2-2 and 1-3 structures

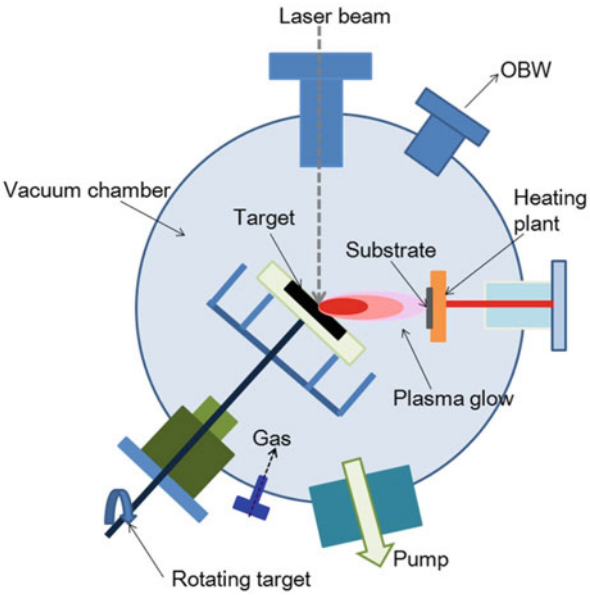

Fig. 14.3 A sketch of pulsed laser deposition (PLD) system

14.3.1 Synthesis Method

Researchers have synthesized FE/ferromagnetic, manganite/metal oxide, superconductor/metal oxide, DE/metal oxide, and CD oxide/noble metal nanocomposite films with nanogranular, nanolayer, nanocolumnar and nanocheckerboard configurations via physical deposition techniques (e.g., pulsed laser deposition (PLD), magnetron sputtering, molecular beam epitaxy (MBE)) and chemical method (e.g., sol-gel method). Among these method, PLD is a widespread technique for well-controlled epitaxial growth of complex oxide films (Fig. 14.3). Here, we just describe three important methods to synthesize nanocomposite films that are based on the PLD technique. The first, templated self-assembly of functional oxide nanocomposites films have been applied to synthesize nanocompostie films with nanocolumnar structures. The second, a single composite targets is used to deposit nanocomposite oxide film with different microstructure. The third, two targets with the single phase are used to deposit nanocomposite oxide film with different microstructure.

14.3.1.1 Template

Templating of the locations and geometry of the self-assembled columnar would dramatically increase the utility of the nanocomposite oxide films. Seeding the nucleation of the nanocolumnar was first demonstrated for 100–200 nm period, 20–30 nm thick BFO/CFO nanocomposites grown by pulsed electron deposition on

a substrate patterned with CFO seed particles made from a CFO film by electron beam lithography and ion milling [26]. Aimon et al. using a new method for templating BFO/CFO nanocomposites based on selective nucleation in topographc feature produced in the substrate by either top-down focused ion beam irradiation or wet etching through a self-assembled triblock terpolymer mask. In this procedure, the second phase of CFO shows enhanced aspect ratio and large magnetic anisotropy [27]. However, as the technology is pushed to ever-smaller length scale, both the "top-down" lithography and "bottom-up" self-assembly methods used to fabricated nanostructures becomes increasingly challenging. Self-assembly process using single composite target and two target with single phase have attract tremendous attention for creating a range of nanoscale structure types [28, 29].

14.3.1.2 Single Target

For the one single composite targets, the self-assembly mechanisms of oxide nanocomposite films, as well as the advantageous of Self-organization are important to modulate the microstructure of the films. In order to predict new compositions one need to select systems that have the potential to undergo these spinodal processes. The kinetic and thermodynamic parameters are a guide to this selection [15]. For example, Bi_2FeMnO_6 with supercell structure have been prepared using the composite target in which compounds Bi_2O_3, Fe_2O_3 and MnO_2 were mixed in stoichiometric ratio [30]. Chen et al. also synthesized $La_{0.7}Sr_{0.3}MnO_3$/ZnO (LSMO/ZnO) nanoculomnar structures using the $(LSMO)_{0.5}/(ZnO)_{0.5}$ composite target [31]. The main challenge for single composite target method is to create structures of the desired compositions. Since the compositions rely on phase separation from a single starting composition, achieving the desired compositions is harder than for standard multilayer growth where each individual composition is grown from a separate target.

14.3.1.3 Two Targets

For the two targets with single phase, deposition is always carried out from two targets sequentially, producing submonolayer films from each target to ensure intermixing of the film [32–34]. The target was rotated sufficiently fast to ensure that much less than one unit cell was deposited per one rotation so that complete intermixing of the two constituents could take place [35]. For example, Imai et al. have epitaxially grown $Bi_4Ti_3O_{12}$ (BTO):CFO nanocomposite films using BTO and CFO single targets which were either simultaneously or alternatively deposited on 0.5 wt.% Nb-doped STO (001) (Nb:STO) by PLD [36]. Zhao et al. Have successfully synthesized composite films with nanocolumnar configurations in the LSMO/V_2O_3 (VO) system. The average deposition fluxes for LSMO and VO at this condition are 2 Å/min and 1.3 Å/min, respectively. To grow LSMO/VO

nanocomposite, LSMO and VO targets were alternately switched in situ to the deposition position for certain amount of time for the deposition with LSMO grown first on the substrate [37]. A dual target technique [38] has also been employed to synthesize CFO/$SrRuO_3$ nanostructured thin films [39]. Using the two targets systems, the nanocomposite thin films with nanogranular, nanomultilayer, nanocolumnar and nanocheckerboard configuration have been successfully in the LSMO:NiO and $La_{0.7}Ca_{0.3}MnO_3$:NiO (LCMO:NiO) [4, 5]. For example, as shown in Fig. 14.4. to produce the LCMO:NiO composite films, two separated targets of

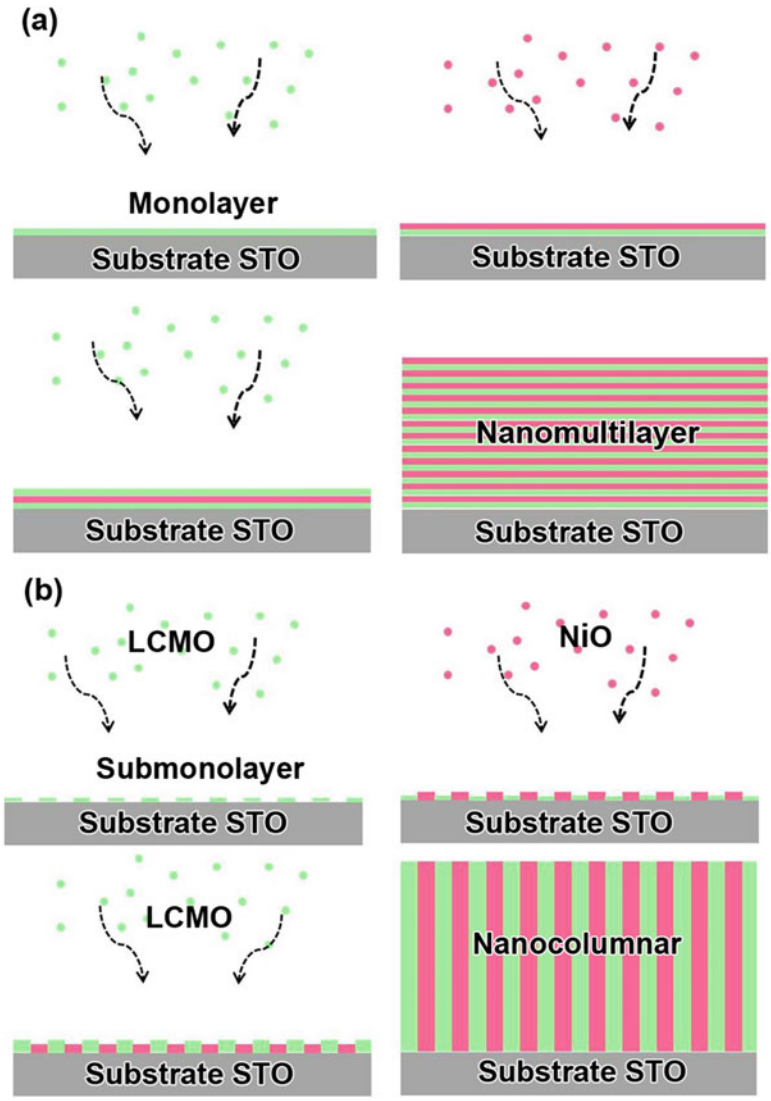

Fig. 14.4 Schematic illustrations of the growth modes for the LCMO:NiO composite films with equal volume fractions of LCMO and NiO but with different microstructures: (**a**) nanomultilayer configuration and (**b**) nanocolumnar configuration [5]

LCMO and NiO were alternately used to deposit LCMO and NiO on the STO substrate. By controlling the deposition time for LCMO and NiO, LCMO:NiO nanocomposite films with the configurations of nanocolumnar, nanogranular and nanomultilayer have been formed [5].

14.3.2 Microstructure

14.3.2.1 Nanogranular (0-3 Structure)

In this kind of nanocomposite structure, The physical properties such as the magnetoelectric coupling (MEC), DE, magnetoresistance and electrical conductivity have been effectively improved. For example, Bi et al. fabricated a CD composite film of $LaNiO_3$/Pt with the nanogranular configuration by radiofrequency co-sputtering. The conductivity of the composite films enhanced compared with the pure $LaNiO_3$ films [40]. Wan et al., Zhang et al. and Ryu et al. have prepared Pb(Zr, Ti)O_3(PZT)/CFO, (x)$Bi_{3.15}Nd_{0.85}Ti_3O_{12}$/(1-$x$)CFO and PZT/NiFe2O4 (NFO) composite films with nanogranular configuration, the values of the magnetic coupling coefficient increased compared with the single phase of the multiferroics material [41–43]. However, in the nanogranular structures, the low resistivity of the interface between the spinel phase and the perovskite parent phase form a CD paths across the films, resulting in severe leakage of the films and the FE properties were dramatically decreased or disappeared. Staruch et al. have synthesized $La_{0.67}Sr_{0.33}MnO_3$:MgO nanocomposite films with La, Sr, Mn, and Mg were mixed in stoichimetric ratio 0.67/0.33/1/x. Curie temperature and metal-insulator transition temperature systematically decrease with increasing molar concentration of Mg(O). Low-field magnetoresistance (LFMR) of films significantly enhanced by Mg addition, values were ~35.5% and ~83.2% respectively [44, 45].

In summary, the composite films with nanogranular configuration can effectively improve the magnetoelectric coupling effect, conductivity and the magnetoresistance, but have an adverse effect on the FE properties in the multiferroic composite films.

14.3.2.2 Nanomultilayer (2-2 Structure)

PLD and the magnetron sputtering have been widely used for preparing the nanocomposite oxide film with nanomultilayer configuration. Generally, the low-resistivity phase could be completely isolated by the high-resistance phase, resulting in high resistance for the composite films with nanomultilayer configuration. Under this circumstance, the nanocomposite films with nanomultilayer configuration can effectively improve the leakage in the multiferroic composite film and also can enhanced the FE and DE properties in the corresponding composite films. In addition to this, the LFMR in the manganites based composites films also

improved in this microstructure [46]. Ma et al. and Deng et al. synthesis BTO/CFO and BTO/NFO layered structure and measured the response of the FE and ferromagnetic coupling coefficient, showing an enhanced magnetoelectric coupling properties compared with the nanocomposite with the nanogranular configuration [47, 48]. Recently, researchers have found that by minimizing the thickness of each layer in the nanomultilayer structure one can increase the areas of the interface, leading to enhanced coupling properties and also explore novel physical properties. For example, Dawber et al. synthesised a FE/DE superlattices and showed that the FE properties is dramatically improved. Novel physical properties also have been found in this system such as the novel polarization reversal mode [49, 50]. In FE superlattices, modulating the periodic thickness is a flexible and efficient method to regulate the physical properties [51, 52]. Hesse et al. showed that a remarkable enhancement in polarization and DE constants, and unusual ferroelectricity have been observed in ferroelectric superlattices which are expected to be used in the preparation of high-performance microelectronic devices [53, 54].

In summary, compared with the nanogranular configuration, nanocomposite oxide films with the nanomultilayer configuration can effectively improve the physical properties such as magnetoelectric coupling in multiferroic system and LFMR in manganites composite film.

14.3.2.3 Nanocolumnar (1-3 Structure)

Recently, there has been significant interest in the design and development of the the nanocomposite oxide films with nanoculomnar configuration due to the exciting prospects for next generation devices in data processing and storage [55]. PLD and template methods have been widely used to synthesis the composites films with nanocolumnar configuration. Compared with the lateral interface of, the effect of vertical interface on the physical properties of metal oxide films is profound [56]. The dominant strain mechanism for the two phase in the nanocolumnar structure arises from the vertical interface, rather than from the lateral interface which are much larger than the pure films of the two phase. It is noted that the vertical interface is more efficient to control the out-of-plane lattices constant than the lateral interface [57], particular in the relatively thick composites films. The long-range strain field across the films can effectively tune the physical properties which could be used to modulated the functionalities of the composite films. For example, Zhao et al. have precisely tuned the microstructure of the $(YBa_2Cu_3O_{7-\delta})_{1-x}/(BaZrO_3)_x$ (YBCO/BZO), and the Curie temperature of the YBCO have been widely tuned for the microstructures with the nanocolumnar configuration [11]. Yang et al. have investigated the vertical interface effect on the physical properties of epitaxial BFO/Sm_2O_3 (BFO/SmO) nanocomposite films. The nanocomposite shows a lower than expected DE loss, due to the presence of a larger vertical interfacial area in the nanocomposite, causing a reduction of the oxygen depletion in the BFO phase relative to a pure BFO film [56, 58]. In addition, MacManus-Driscoll et al. and Ning et al. have prepared LSMO:ZnO and LSMO:NiO composite films with nanocolumnar configuration.

The value of the LFMR have been largely enhanced due to the strong electron scattering at the ferromagnetic/insulator interfaces and magnetic tunnel junctions (MTJs) of LSMO/insulator/LSMO at the nanometer scale [4, 6, 31].

In summary, compared with the nanocomposite films with the nanogranular and nanomultilayer configuration, nanocolumnar structure shows large advantage in multiferrotic based and manganite base composite films by tuning the DE and LFMR properties.

14.3.2.4 Nanocheckerboard (0-0 Structure)

One major challenge for further enhancing the LFMR in a high temperature range in the manganites based composite films is how to tune the crystalline grain size of the second phase. It is also noted that in the manganites based composite thin films, if manganites phase contacts with an insulator phase and then other manganites phase forming a manganites/insulator/manganites structure, a magnetic tunneling junction (MTJ) can be formed. The MTJs of manganites/insulator/manganites are important to enhance the LFMR properties of composite films. To achieve this object, the major challenge is how to control the grain size of the insulator phase within 1–2 nm, which is the optimized thickness of a middle layer in a MTJ structure [59, 60]. As have been mentioned in the method section, the nanocheckerboard oxide films which are formed by pseudo-spinodal decomposition shows controllable grain size within 10 nm. MacManus-Driscoll et al. have reported the in-plane nanocheckerboard-like structure in the LSMO:ZnO nanocolumnar structure (nanocheckerboard configuration along the in-plane direction, but nanocolumnar configuration along the out-of-plane direction.) [15]. Although, the values of the LFMR are largely enhanced in the low-temperature range, but rapidly decreased near the Curie temperature. In 2014, nanocheckerboard configuration along the out-of-plane direction have been successfully synthesized at the first time by Ning et al. [4], as shown in Fig. 14.5. The composite films with the checkerboard-like structure exhibit a large LFMR in the high temperature range from 200 to 300 K with the highest value of 17% at 250 K under a magnetic field of 1 T.

14.4 Nanocomposite Films and the Potential Application

14.4.1 Multiferroic Nanomposite Film

For the multiferroic composites, which incorporate both ferri-/ferromagnetic (FE/FM) phases, typically yield giant magnetoelectric coupling (ME) response above room temperature, makes them ready for technological applications. The availability of high-quality nanostructured composites makes it easier to tailor their properties through epitaxial strain, atomic-level engineering of chemistry, and

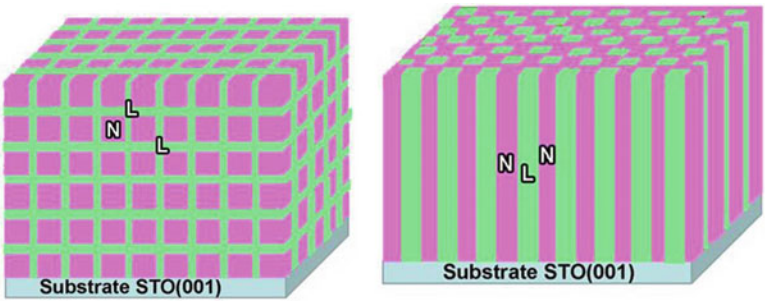

Fig. 14.5 Schematic illustrations of (**a**) the ideal checkerboard-like structure and (**b**) the nanocolumnar structure in the nanocomposite thin films. "L" stands for LSMO phase and "N" stands for NiO phase

interfacial coupling. Of interest, motivated by on-chip integration in microelectronic devices, the coupling interaction between nanosized FE and magnetic oxides nanostructured composites have recently been deposited in a film-on substrate geometry. Thus the ME composites are ready for technological applications. Promising applications include magnetic field sensors thus complementing Hall sensors and current measurement probes, transducer, filters, oscillators, phase shifters, memory devices, and so on [61]. Figure 14.6 shows a sketch of the ME gyrators and the equivalent circuit which have important applications as voltage gain devices, current sensors, and other power conversion devices. An extremely high voltage gain effect under resonance drive has been reported in long-type ME laminates consisting of Terfenol-D and PZT layers [62].

Recently, perpendicular recording technology has been introduced in hard disk drives, as the traditional longitudinal recording technology is approaching its storage limit due to superparamagnetic effects. Large and well controlled magnetic anisotropy in nanocolumnar FE/FM compostite films is thus necessary to guarantee bit stability, while preserving high density storage capability [63]. Integration of nanocomposites on a Si platform would provide a path towards large scale and low cost devices such as multiferroic memory and logic. Integration of self-assembled epitaxial BFO/CFO multiferroic nanocomposites on silicon substrates have now been successfully synthesised by Kim et al. [64].

In 2004, Zheng et al. have firstly synthesis BTO/CFO naocompsoites films with nanocolumnar structure by PLD, in which CFO formed prismatic columns which extended from the substrate to the top surface, embedded in a BTO matrix [1]. Since this pioneering work, the nanocomposite films in this systems with the structure of nanoculumnar configuration have been widely reported due to the higher magnetoelectric coupling than their laminate counterparts and the nanogranular structures [65–68]. Figure 14.7 shows the typical SEM images of the BFO/CFO nanocomposite films with nano columnar structures reported by Dix et al. [69].

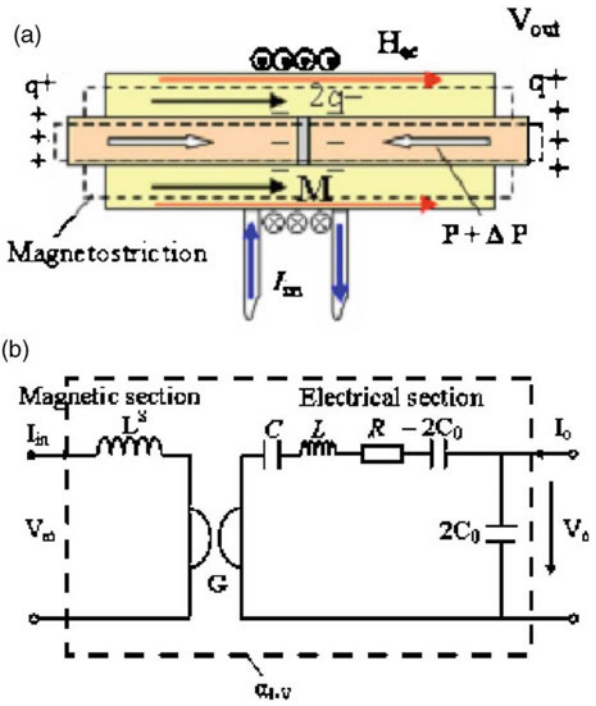

Fig. 14.6 (**a**) a sketch of the ME gyrator (**b**) ME gyration equivalent circuit [62]

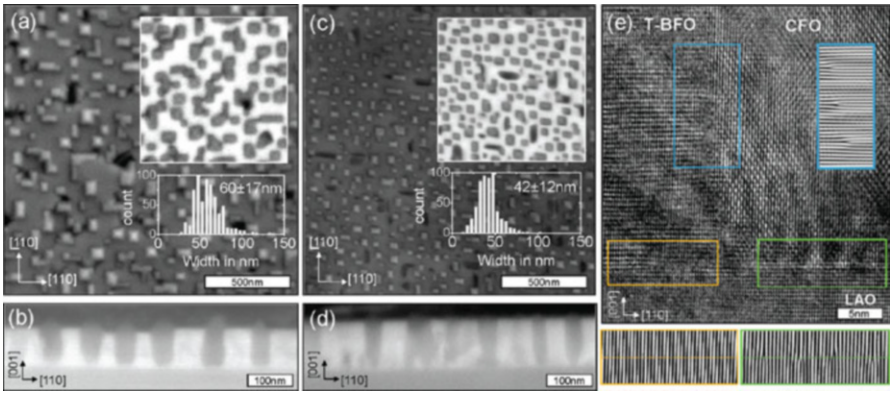

Fig. 14.7 SEM images (secondary electrons) of BFO/CFO on $LaNiO_3$ (LNO)/$LaAlO_3$ (001). The area in the top right inset was imaged with backscattered electrons[69]

In this systems that have nanoculomnar configuration thus far, the ferromagnetic material is chosen from the AB_2O_4 spinel family (such as CFO or NFO) and the FE materials is chosen from ABO_3 perovskite (such as BFO, BTO, and $PbTiO_3$), respectively [36]. In this nanoculmnar configuration, whereas the resistive CFO pillars exhibited single-domain magnetic contrast with high anisotropy due to the

magnetoelasticity of the spinel phase. Magnetoelectric coupling was observed in which an applied voltage led to reversal of the magnetic pillars [3].

However, in nanocomposites on STO (001), the spontaneous polarization of BFO is at around 55° with respect to the normal direction, whereas in the CFO nanopillars the out-of-plane is the magnetic easy axis. Clearly, the fixed directions of the FE and FM easy axes in a columnar nanocomposite restrict its development for optimal exploitation of both ferroic properties and magnetoelectric response [36]. Dix et al. demonstrate that epitaxial strain engineering is an efficient method to manipulate the ferromagnetic and FE properties in BFO/CFO columnar nanocomposites [36]. On the one hand, indeed, electric-field induced switching of magnetization has been observed, at room-temperature, in CFO nanopillars in BFO matrix deposited on STO (001) [2, 70, 71] and it is believed that elastic interaction mediates the magnetoelectric coupling [61]. On the other hand, Wang et al. report growth of various phase architectures of self-assembled BFO/CFO thin films on differently oriented STO substrates. CFO forms segregated square, stripe, and triangular nanopillars embedded in a coherent BFO matrix on (001)-, (110)-, and (111)-oriented STO substrates, respectively. Nanostructures with an aspect ratio of up to 5:1 with a prominent magnetic anisotropy were obtained on both (001) and (110) STO along out-of-plane and in-plane directions. Magnetic easy axis rotation from in-plane to out-of-plane directions was realized through aspect ratio control [72]. This paper will pave the way on the perpendicular recording technology as the well controlled magnetic anisotropy in this nanocolumnar FE/FM compostite films.

The recent progress in the multiferroic nanocomposites films not only provide a strategy for producing a new class of delicately functional materials, but also shed promising light on fabricating the ME part of the devices. In the future, the possibility of further tuning the electric polarization or magnetization of the multiferroic nanocomposites films should be evidenced by the coupling and charge transfer of the 3*d* ions at the phase interfaces.

14.4.2 Manganites Nanocomposite Film

Lanthanum manganite perovskites $La_{1-x}A_xMnO_3$ (A is a divalent cation) with a Curie temperature (T_C) above room temperature (LSMO) or with the T_C below room temperature (LCMO) have attracted great attention due to their complex magnetic properties and the colossal magnetoresistance (CMR) occurring around the T_C [73, 74]. These CMR materials are particularly interesting as designing the memory-readers of digital device, magnetic sensor, p-n junctions or spintronic applications involving GMR effect with the high-T_C superconductivity (Fig. 14.8) [75–77]. However, on the one hand, the intrinsic CMR value in this system can only be triggered at a high magnetic field of several Teslas and within a narrow temperature range [78], which obstructed applications such as magnetic head sensors or low-cost magnetic sensors that should be operated at a low magnetic field and stable temperature-sensitive environment [79, 80]. On the other hand,

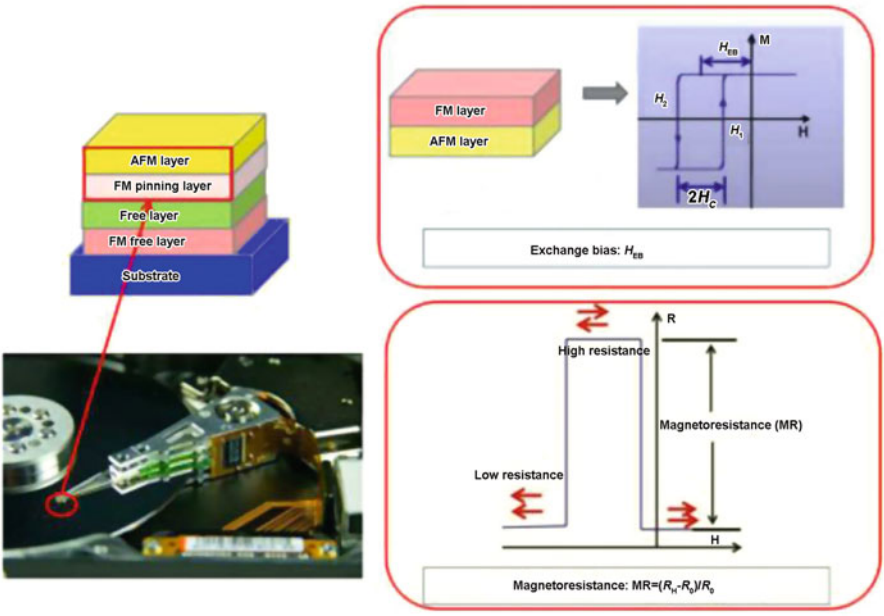

Fig. 14.8 A sketch of the magnetic head sensor and the magnetoresistance effect

lower temperatures of the metalinsulator transition and the magnetoresistance enhancement at low temperatures were obtained by reducing the manganite film thickness or by creating manganiteinsulator superlattices with periods of $n \leq 10$ [81]. However, few observations of unusual CMR behavior in these superlattices were reported below 90 K, the range of interest for combination with high-temperature superconductivity (HTS) materials [46].

14.4.2.1 LSMO Nanocomposites

Recently, due to the deepening cognition of the intrinsic and extrinsic CMR effect, attention has been paid to polycrystalline manganites to obtain the extrinsic low-field magnetoresistance (LFMR) by structuring grain boundaries, nanosized inclusions, interface phase, and artificial grain boundaries. What's more, the LFMR in composites or films can be further improved by introducing a secondary phase (usually non-magnetic or antiferromagnetic insulators) [37, 82–84]. For example, the LFMR values of −6% at 5 K and 0.16 T in LSMO/STO nanomultilayer structure [73], −17.5% at 30 K and 1 T in LSMO:ZnO nanocolumnar structure [31], −8% at 10–150 K and 1 T in LSMO/MgO nanorod arrays structure [85], −12% at 77 K and 0.4 T in LSMO/Ag nanogranular structure [86] and −17% at 250 K and 1 T in LSMO/NiO nanocheckerboard structure [4] have been reported. Figure 14.9 shows the LFMR properties for the LSMO based composites.

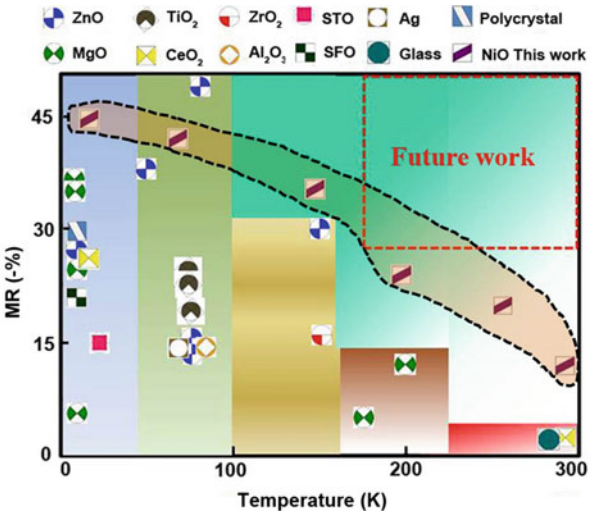

Fig. 14.9 Temperature range of the LFMR for the LSMO composites.NiO: refs [4, 5], ZnO: refs [87, 88], MgO: refs [85, 89, 90] , TiO_2: refs [91–93] , CeO_2: ref [94] , ZrO_2: ref [95] , Al_2O_3: ref [88] , STO: ref [96] , SFO: ref [97] , Ag: ref [88] and glass: ref [98]

However, neither the early results obtained from LSMO polycrystalline films or recent results obtained from LSMO/ZnO composite films with a nanocolumnar structure [31], enhanced LFMR values are always displayed in a low temperature range (below room temperature). Systems featuring a large LFMR at temperatures close to or even higher than room temperature are more important owing to their potential applications in magnetic field sensing and data storage [99]. However, no LFMR properties above room temperature have been reported until now. As shown in Fig. 14.7, compared with other microstructures, more research has been carried out on nanomultilayer and nanocolumnar configurations as the significant enhancement of the LFMR at high temperatures range, for example, in the LSMO/MO system (where MO is a binary metal oxide, such as NiO, CeO_2, ZnO, and VO, etc.) [44, 57, 87, 97, 99–104]. Dey et al. have found that the large LFMR will keep steady in a higher temperature range when the grain size is in nanoscale and gets with the decrease in particle size [100]. It is that the spin pinned effect occurs at the nanosized grain surface defect sites or spin coupling at the boundaries. In addition, the short range FM coupling order may add the opportunity of spin scattering even near the Curie temperature. Thus it is speculated that the high-temperature LFMR in LSMO composite films can be got through tuning the grain size and the FM coupling at the phase boundary. Under these circumstances, the future work should be done for the nanocompsoite films with interfacial FM coupling.

14.4.2.2 LCMO Composites

As have been mentioned above, LFMR behavior in the LCMO based composite films were also important below 90 K, the range of interest for combination with HTS materials [46]. Recently studies have shown that the MR% values (>80% at a

magnetic field of 1 T) in the nanomultilayer films are much higher than those previously reported in the LCMO-insulator composites such as LCMO/MgO (20%, 1 T) [106], LCMO/BTO (30%, 1 T) [107], LCMO/STO (70%, 2 T) [108] and LCMO/ZnO (18%, 0.5 T) [109]. Ning et al. have reported that the LCMO/NiO nanocomposite films with nanomultilayer, nanogranular and the nanocolumnar microstructures show a flat plateau in the LFMR versus temperature curves [5]. The experimental results of the LCMO based nanocomposite films demonstrated that the LFMR values and temperature range of self-assembled nanocomposite films can be effectively modulated by tuning their microstructures. In addition to this, to modulate the geometry distribution of these nano-sized phases may favor the artificial designing of the LFMR properties. For the composite films, the small size and large aspect ratio of nano-structure insulator phase would favor the LFMR, because the insulator tunneling barriers and the scattering centers at the phase interface with reducing the grain size of the insulator phase. Actually, the LCMO base nanocomposite films with different microstructure can be explained within the framework of a Resistance–capacitance (R_C) and series circuit model [4, 46], arising as a result of the well-ordered 3D geometric shapes and arrangements of the LCMO and the second phases in the composite films, as shown in Fig. 14.10 [4].

However, the unusual plateau in the LFMR versus temperature curves in LCMO based composites films makes the high LFMR values remain up to a sufficiently higher temperature of approximately 100 K. More importantly, the unusual flat plateau region in the LFMR versus temperature curves implies a broadened temperature range for potential applications in field sensor devices, especially for the

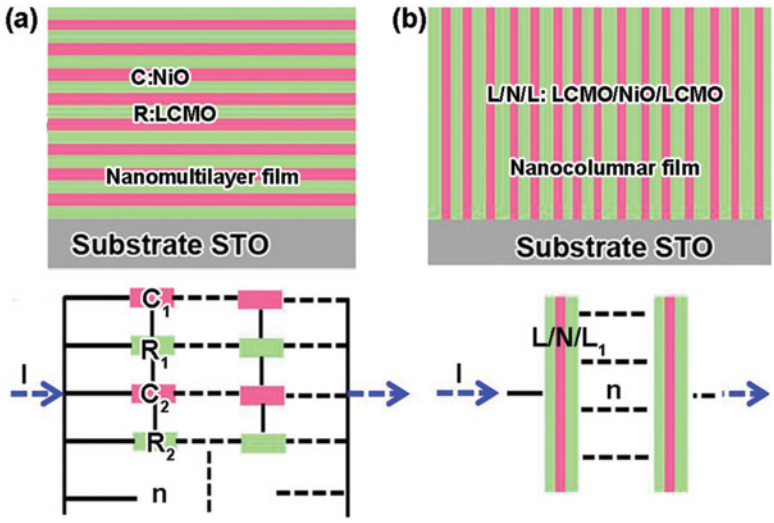

Fig. 14.10 Schematic illustrations of a simple circuit model for (**a**) the nanomultilayer structure and (**b**) the nanocolumnar structure [4]

heterostructures composed of cuprate and manganite components that are used for spintronic applications employing LFMR and HTS.

14.4.2.3 Conclusion

To sum up, the LFMR of the manganites based nanocomposites films can be effectively modulated by tuning the microstructure. On the one hand, the LFMR on the LSMO based nanocomposite thin films with the T_C above room temperature can be used as the memory-readers of digital device. On the other hand, the LFMR on the LCMO based nanocomposite thin films with the T_C below room temperature can be used for spintronic applications employing LFMR and HTS. However, significant challenges still need to be overcomed before manganites nanocomposite films based devices become a reality.

14.4.3 Superconductor Nanocomposite Film

Recently, the superconductor based nanocomposites oxide films have been studied extensively. On the one hand, the coupling between the antagonistic superconducting (SC) and FM orders in thin film multilayers is the subject of intensive research [110]. The proximity effect at superconductor-ferromagnet interfaces produces damped oscillatory behavior of the Cooper pair wave function within the ferromagnetic medium. In 2003, Ustinov et al. proposed using the π junction as a phase shifter in rapid single flux quantum circuits. The π junctions can scale the dimension of superconducting logic circuits down to the submicron size [111]. The structures consisting of 0 and π Josephson junctions are also very important to design phase based devices. The exchange interaction between the SC and FM could strongly affects Andreev reflection at the F/S interface which could providing a powerful tool to probe ferromagnets and measure their spin polarization [112]. On the other hand, special attention is paid to the striking nonmonotonic dependence of the critical temperature and the magnetic-flux pinning based device in the SC nanocomposite films also have been well studied.

14.4.3.1 YBCO:LCMO Nanomposites

The pioneering work on spin-polarized transport in conventional superconductors has been recently extended to high transparency ferromagnet-superconductor heterostructures where the two-particle process of Andreev reflection plays an important role [113–115]. The role of Andreev bound states across a YBCO/LSMO interfaces have been reported by Chen et al. [116]. The suppression of Andreev bound states in the a-b plane by the spin-polarized transport across the interface consistent with the reported photoemission data. In 2004, Holden et al.

have studied the proximity induced metal-insulator transition in YBCO/LCMO nanomultilayers and suggest that either a long-range charge transfer from the YBCO to the LCMO layers or alternatively a strong coupling of the charge carriers to the different and competitive kind of magnetic correlations in the LCMO and YBCO layers is at the heart of the observed metal-insulator transition [117]. In 2005, Hoffmann et al. studied the magnetic properties of YBCO/LCMO nanomultilayer using the polarized neutron reflectometry and shown that the magnetization is reduced due to an inhomogenous magnetization depth profile arising from the suppression of magnetization near the YBCO/LCMO interface [118]. After then, the magnetic proximity effect at the YBCO/LCMO interface of the composite films is becoming an increasingly important issue [119–121]. They have demonstrated that in such a heterostructure the inhomogeneous exchange field enhances the proximity effect. Satapathy et al. shows that the magnetic proximity effect strongly depends on the electronic state of the manganite layers, being pronounced for the ferromagnetic-metallic LCMO and almost absent for ferromagnetic-insulating $LaMnO_3$ [110]. The charge transfer effect from Mn to Cu and the orbital reconstruction across the interface are important factors in determining the proximity effect of this heterostructure [122]. However, De Luca et al. show that, even in the absence of direct Cu-O-Mn covalent bonding, the interfacial CuO_2 planes of superconducting $La_{1.85}Sr_{0.15}CuO_4$ thin films develop weak ferromagnetism associated to the charge transfer of spin-polarised electrons from the $La_{0.66}Sr_{0.33}MnO_3$ ferromagnet [123]. Chien et al. studied the buried interfaces between cuprate and manganite layers using cross-sectional scanning tunnelling microscopy and spectroscopy together with atomic-resolution electron microscopy. The results show that the fundamental length scale of the electronic evolution between YBCO and LCMO is confined to the subnanometre range [124].

14.4.3.2 YBCO:BaZrO3 Nanomposites

In 2005, MacManus-Driscoll et al. have found a strongly enhanced current densities in superconducting coated conductors of YBCO/$BaZrO_3$ (BZO) [125]. They also have pointed out that by changing different types of heteroepitaxial addition and concentration, it is likely that other concentrations and different heteroepitaxial second-phase additions will lead to yet greater enhancements in pinning. Then after, the YBCO based nanocomposite films with different microstructure have been widely explored. Kang et al. have found an enhancements of the critical current in self-field as well as excellent retention of this current in high applied magnetic fields in the thick films via incorporation of a periodic array of extended columnar defects, composed of self-aligned nanodots of nonsuperconducting material extending through the entire thickness of the film. These columnar defects are highly effective in pinning the superconducting vortices or flux lines, thereby resulting in the substantially enhanced performance of this wire [126]. Depending on the angle-dependent critical-current measurements, Gutiérrez et al. demonstrates that a strong and isotropic flux-pinning mechanism is extremely effective at high

temperatures and high magnetic fields leading to high-temperature superconductors with record values of pinning force (65 K, 78 GN m^{-3}) [127]. However, retaining a dissipation-free state while carrying large electrical currents is a challenge that needs to be solved to enable commercial applications of high-temperature superconductivity. In 2009, Maiorov et al. show that the controlled microstructures is possible and effective which is used to produce thick films with remarkable IC (H) and nearly isotropic angle dependence [128]. Recent studies are then focus on the microstructure of the YBCO based composites films and the corresponding functional properties, especially for the critical temperature [129, 130]. In 2014, Zhao et al., have realized the precise tuning of the microstructure from vertical nanocolumnar structure to horizontal nanomultilayered in the YBCO/BZO systems [11], as shown in Fig. 14.11.

14.4.3.3 Conclusion

The concept of combining materials with superconductors in the form of artificially grown nanocolumnar and nanomultilayer can be useful in advancing our fundamental understanding of superconductive properties and the way they change with the addition of nanosized correlated defects and second phases. The flux pinning and critical current can be readily tuned with the shape, order, and size of embedded nanoparticles. The future challenge is explore the subtle changes in interfacial composition and coupling effect at the phase interfaces.

14.4.4 Ferroelectric, Dielectric and Conductive Nanocomposite Film

FE, DE and CD oxides incorporating 3*d* transition metals, in particular ABO_3 perovskites, have been fertile ground for the discovery and application in the electronic industry. For example, BTO, $Pb(Zr_xTi_{1-x})O_3$ (PZT), $(1-x)Pb(Mg, Nb)O_{3-x}PbTiO_3$ (PMN-PT), LNO etc. which show excellent piezoelectric, DE, FE, pyroelectric and CD properties have been widely used in the sensors, capacitors, nonvolatile memory, surface acoustic wave devices and electrode for the microelectronic devices (Fig. 14.12). These three nanocomposite material are the key materials for the FE random access memory (FRAM) and microelectro-mechanical systems (MEMS).

Recently, remarkable improvement in oxide thin-film techniques have allowed for the growth and characterization of complex oxide heterostructures with (near) atomic precision, opening an avenue for the fabrication of the composite films with different microstructures which shows high polarization performance FE composite

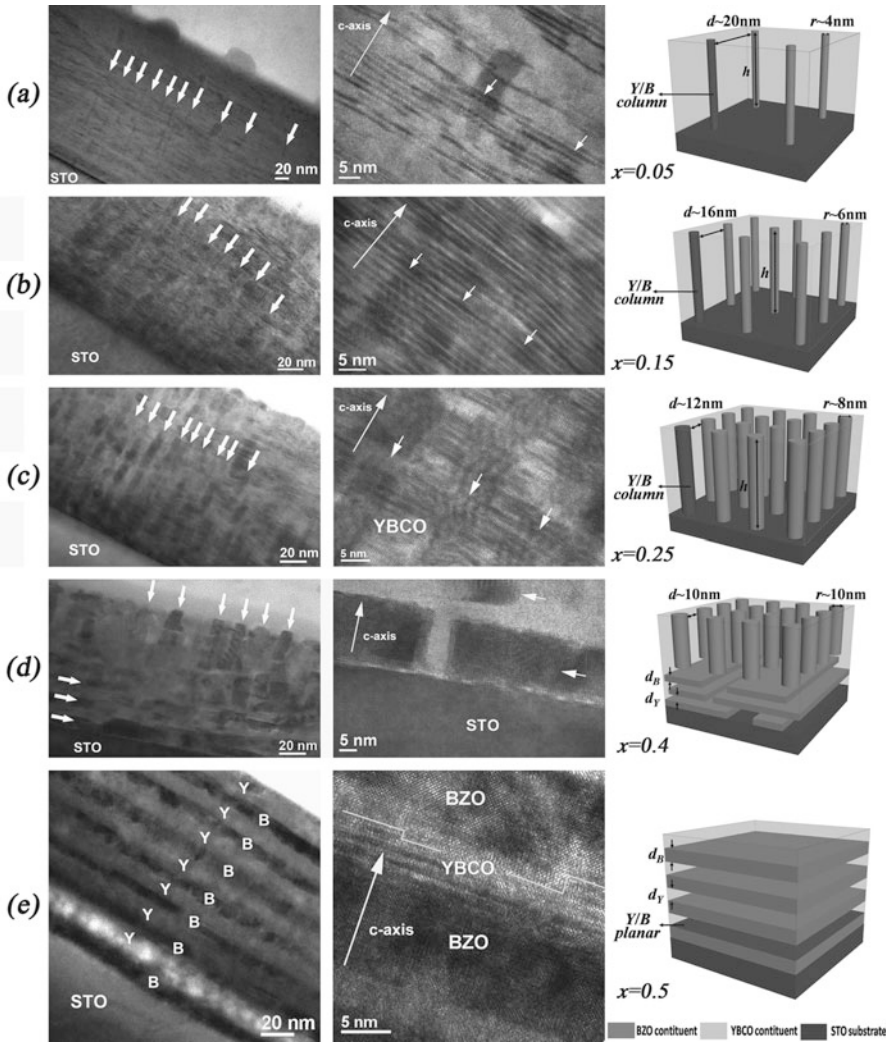

Fig. 14.11 Cross-sectional TEM images of YBCO/BZO thin films with different microstructure [11]

films, high DE properties for the DE composite films and low resistivity for the CD composite films, leading to the rapidly development of the research in the field of FRAM devices.

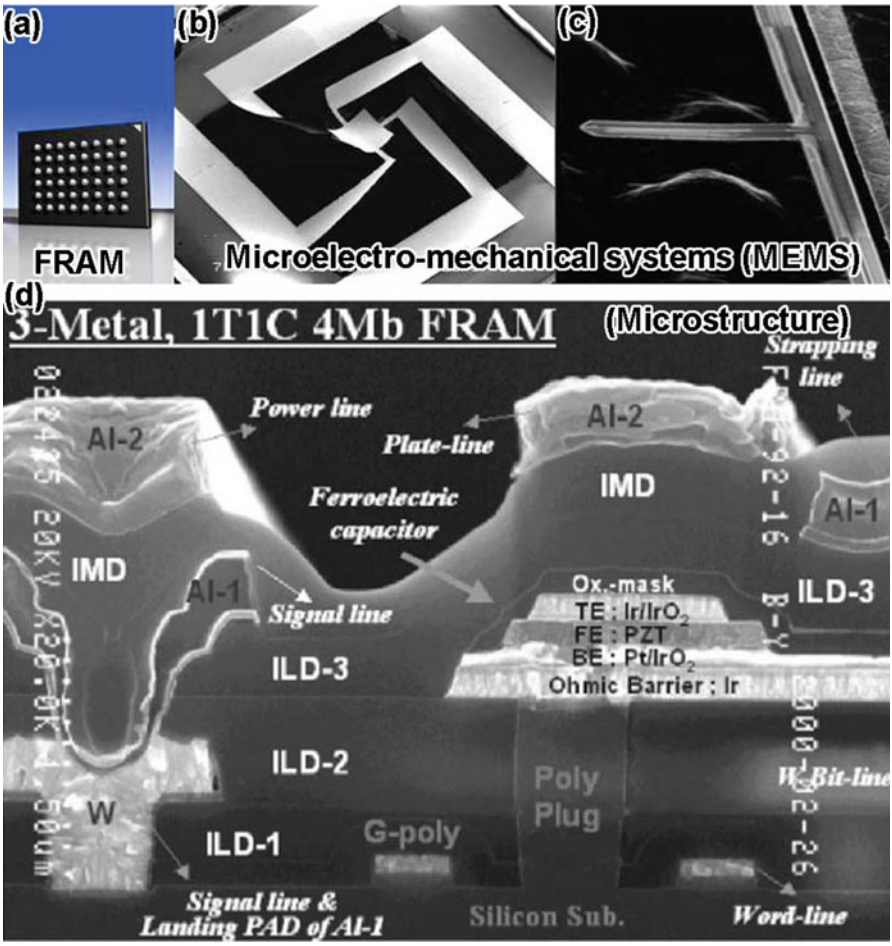

Fig. 14.12. (**a**) the FE random access memory (FRAM) (**b**) and (**c**) Microelectro-mechanical systems (MEMS) (**d**) the corresponding microstructure of the FRAM

14.4.4.1 FE Nanomposites

In this part, we focus on the FE nanocomposite films with nanomultilayer configuration. As have been mentioned above, a remarkable enhancement in polarization and resistivity, and unusual ferroelectricity have been observed in FE superlattices which are expected to be used in the preparation of high-performance microelectronic devices [131–133]. Recently, artificial FE composites films with the nanomultilayered configuration have drawn considerable attention. [134, 135]. The FE nanocomposite films with nanomultilayer configuration have the periodic structures containing different kinds of FE materials. The FE nanomultilayer films can be simply divided into symmetric and asymmetric superlattices according to the

thickness of the two component. In 1994, Tabata et al. have firstly synthesis BTO/STO naocompsoites films with nanomultilayer structure by PLD, in which BTO and STO formed layered structure and epitaxially grown with each other [136]. Since this pioneering work, the nanocomposite films in this systems with the structure of nanomultilayer configuration have been widely reported due to the excellent polarization performance. As compared to the their corresponding counterparts epitaxially grown on the substrates, which have been already extensively studied, the strain is one of the most important issues to modulated the FE properties. The theoretical dependence of the properties of FE films with different states have been studied extensively [137, 138]. Ederer et al. Have show that the epitaxial strain dependence of the polarization varies considerably for the different systems, and in some cases is, in fact, very small [139]. The strain state can be simply controlled by selecting the substrates with different lattice parameters. There are some scientific papers report on strain dependency of the nanomultilayers on various substrates and shows that the FE and piezoelectric behavior is consistent with the theoretical model for the films with different strain states [140–143].

14.4.4.2 DE Nanomposites

Recently, on the one hand, composite thin films of metal-perovskite oxides have produced a tremendous flurry of research interest because of their unique physical and chemical properties. Ge et al. Have shown that the Co and Ni nanocrystals in the face-center cubic structure dispersed well in the single BTO matrix monitored by in situ reflection high energy electron diffraction. Their results provide an efficient way to engineer BTO/Ni or BTO/Co nanocomposite films with desired qualities [144, 145]. Metal-DE nanocomposite films, such as BTO/Co, BTO/Au and $PbTiO_3$/Pb (PTO/Pb) composite films, have showed enhanced optical and electrical properties [8, 9, 146] On the other hand, composite thin films of DE:metal-oxides have also been studied extensively as the low leakage and the enhanced DE properties. Lee et al. have studied the $Ba_{0.6}Sr_{0.4}TiO_3/Sm_2O_3$ (BSTO:SmO) nanocomposite films with nanocolumnar structure. They created a nanoscaffold composite which has a very high tunability which scales inversely with loss. Furthermore, low DE loss values of <0.01 significantly lower than reference pure films (Fig. 14.13) [147]

14.4.4.3 CD Nanomposites

Adding metal nanoparticles into the CD oxide could also reduce the resistivity of the composite films. For example, Tin doped indium oxide films (ITO) with embedded silver nanoparticles were prepared by Boen et al. [148]. Delafossite structure of tin doped $AgInO_2$ was found at lower annealing temperatures in all compositions. The interconnected network of Ag phases provides effective

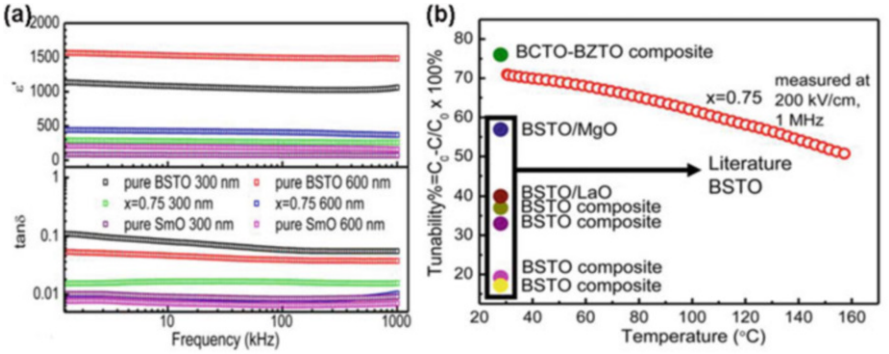

Fig. 14.13 (**a**) Relative permittivity, ε', versus frequency (*upper*) and loss tangent, tan δ, versus frequency (*lower*) for 300 nm and 600 nm pure BSTO, SmO, and nanocomposite films; (**b**) tunabilities for 600 nm, $x = 0.75$ nanocomposite films as a function of temperature (25–160°C) in comparison to similar thickness BSTO and doped BSTO composite films on different substrates, as well as BCTO-BZTO composite film from the literature

conducting paths that reduced the electrical resistivity. Qiao et al. have synthesis a CD composite film of LNO containing 36.1 at.% Pt by radio frequency co-sputtering. The film consists of two individual phases of separated LNO and Pt. Temperature-dependent resistivity measurement indicates a weak electron–phonon interaction and strong electron-electron scattering in the film [40]. Wang et al. have reported that LNO/Au nanocomposite thin films with an excellent electrical conductivity can be prepared by one-step chemical solution deposition [7]. Metal-CD oxide nanocomposite thin films are regarded as promising electrodes for FE devices to overcome the intrinsic drawbacks of conventional metal or CD oxides electrodes. Wang et al. studied the FE PZT thin films with a thickness of 240 nm were deposited on metal CD oxide nanocomposite LNO/Au electrodes by a sol–gel method. It was observed that the PZT thin films fabricated on the LNO/Au bottom electrode exhibited enhanced ferroelectricity [149].

14.5 Conclusions

This review has mainly discussed the nanocomposite oxide films with different microstructure in the field of multiferroics, manganites, supperconductor, FE, DE and CD. New developments are occurring at a rapid pace, throwing further light onto the intricacies of these materials. The dramatic progress in thin film heterostructure and nanostructure growth has been a key enabler fueling these discoveries [12]. However, until now, there are still significant challenges to be overcome before the nanocomposite oxide films base devices become a reality. For example, it should be noted that PLD method as the main method used in this review does not allow large area fabrication of such composite films and the

nanocomposite structure (nanogranular, nanomultilayer, nanocolumnar and nanocheckerboard) is not maintained after a certain thickness that imposes certain limitations. In addition, the functional properties are degraded when epitaxially grown on Si substrate using the chemical method. Although the enhanced performance have been found on nanocomposite oxides films in the past decades, most of these nanocomposite films with different microstructure are focus on films grown on single-crystal perovskite and perovskite-related oxide substrates, including STO, $LaAlO_3$, $DyScO_3$, $NdGaO_3$, etc., to achieve high epitaxial quality. Such single-crystal substrates are expensive and in small dimension, thus not desirable for large-scale integration of oxide thin films with conventional semiconductor devices. Therefore, it is highly attractive to grow these nanocomposite oxide thin films on traditional semiconductor substrates such as silicon (Si) while maintaining a satisfactory performance in the future.

Another problems in these nanocomposite films have have to be taken into considerations. As a class of emerging nanocomposite, most nanocomposite oxide films are still limited to take the advantage of their bimodal physical properties inherited from their single component counterparts. New functions such as the ME coupling effect, charge transfer and FM interactions due to the strong coupling at the interfaces between the two different phases in individual nanocomposite films are barely explored although performance enhancement of the nanocomposite films compared to their corresponding single-component nanoparticles has been observed in several systems. Under this circumstance, precise characterization of the two component interfaces in the nanocomposites films and comprehensive understanding of the interfacial behaviors are critical to reveal the coupling mechanisms that are responsible for improving the functional properties as well as discovering new properties.

Acknowledgements The authors thank Shufang Wang, Mingjing Chen for collaborations. Xingkun thank the National Natural Science Foundation of China with Grant No. 11604073 and 51372064. The Nature Science Foundation for Distinguished Young Scholars of Hebei University.

References

1. H. Zheng, J. Wang, S.E. Lofland, et al., Multiferroic $BaTiO_3$-$CoFe_2O_4$ nanostructures. Science **303**(5658), 661–663 (2004)
2. F. Zavaliche, D. Hong, H.Q. Chiang, et al., Electric field-induced magnetization switching in epitaxial columnar nanostructures. Nano Lett. **5**(9), 1793–1796 (2005)
3. N.M. Aimon, D.H. Kim, X.Y. Sun, C.A. Ross, Multiferroic behavior of templated $BiFeO_3$-$CoFe_2O_4$ self-assembled nanocomposites. ACS Appl. Mater. Interfaces **7**(4), 2263–2268 (2015)
4. X.K. Ning, Z.J. Wang, Z.D. Zhang, Large, temperature-tunable low-field magnetoresistance in $La_{0.7}Sr_{0.3}MnO_3$:NiO nanocomposite films modulated by microstructures. Adv. Funct. Mater. **24**(34), 5393–5401 (2014)

5. X.K. Ning, Z.J. Wang, Z.D. Zhang, Controllable self-assembled microstructures of $La_{0.7}Ca_{0.3}MnO_3$:NiO nanocomposite thin films and their tunable functional properties. Adv. Mater. Interfaces **2**(15), 1500302–1500311 (2015)
6. B.S. Kang, H. Wang, J.L. MacManus-Driscoll, Y. Li, Q.X. Jia, Low field magnetotransport properties of $(La_{0.7}Sr_{0.3}MnO_3)_{(0.5)}$:$(ZnO)_{(0.5)}$ nanocomposite films. Appl. Phys. Lett. **88**(19), 192514–192517 (2006)
7. H.L. Wang, X.K. Ning, Z.J. Wang, Enhanced electrical conductivity of Au-LaNiO3 nanocomposite thin films by chemical solution deposition. RSC Adv. **5**(94), 76783–76787 (2015)
8. Z.R. Wang, T. Hu, L.W. Tang, et al., Ag nanoparticle dispersed $PbTiO_3$ percolative composite thin film with high permittivity. Appl. Phys. Lett. **93**(22), 222901–222904 (2008)
9. W.D. Wu, Y.J. He, F. Wang, et al., Preparation and characterization of Co-$BaTiO_3$ nanocomposite films by the pulsed laser deposition. J. Cryst. Growth **289**(1), 408–413 (2006)
10. M.L. Hammock, A. Chortos, B.C.K. Tee, et al., 25th Anniversary article: the evolution of electronic skin (e-skin): a brief history, design considerations, and recent progress. Adv. Mater. **25**(42), 5997–6038 (2013)
11. R. Zhao, W.W. Li, J.H. Lee, et al., Precise tuning of $(YBa_2Cu_3O_{7-\delta})_{1-x}$:$(BaZrO_3)_x$ thin film nanocomposite structures. Adv. Funct. Mater. **24**(33), 5240–5245 (2014)
12. L.W. Martin, Y.-H. Chu, R. Ramesh, Advances in the growth and characterization of magnetic, ferroelectric, and multiferroic oxide thin films. Mater. Sci. Eng. R Rep. **68**(4), 89–133 (2010)
13. J.S. Andrew, J.D. Starr, M.A. Budi, Prospects for nanostructured multiferroic composite materials. Scr. Mater. **74**, 38–43 (2014)
14. A. Llordés, A. Palau, J. Gázquez, et al., Nanoscale strain-induced pair suppression as a vortex-pinning mechanism in high-temperature superconductors. Nat. Mater. **11**(4), 329–336 (2012)
15. J.L. MacManuas-Driscoll, Self-assembled heteroepitaxial oxide nanocomposite thin film structures: designing interface-induced functionality in electronic materials. Adv. Funct. Mater. **20**(13), 2035–2045 (2010)
16. H. Zheng, Q. Zhan, F. Zavaliche, et al., Controlling self-assembled perovskite-spinel nanostructures. Nano Lett. **6**(7), 1401–1407 (2006)
17. N.N. Padurow, Mischbarkeit im system rutil-zinnstein. Naturwissenschaften **43**(17), 395–396 (1956)
18. D. Fuks, S. Dorfman, S. Piskunov, E.A. Kotomin, Ab initio thermodynamics of $Ba_cr_{(1-c)}TiO_3$ solid solutions. Phys. Rev. B **71**(1), 014111–014120 (2005)
19. C.L. Zhang, S. Yeo, Y. Horibe, Y.J. Choi, et al., Coercivity and nanostructure in magnetic spinel Mg (Mn, Fe)$_2O_4$. Appl. Phys. Lett. **90**(13), 3123–3126 (2007)
20. B.S. Guiton, P.K. Davies, Nano-chessboard superlattices formed by spontaneous phase separation in oxides. Nat. Mater. **6**(8), 586–591 (2007)
21. S. Park, Y. Horibe, T. Asada, et al., Highly aligned epitaxial nanorods with a checkerboard pattern in oxide films. Nano Lett. **8**(2), 720–724 (2008)
22. B. Zhang, M. Lelovic, W.A. Soffa, The formation of polytwinned structures in Fe Pt and Fe Pd alloys. Scr. Metall. Mater. **25**(7), 1577–1582 (1991)
23. Y.L. Bouar, A. Loiseau, A.G. Khachaturyan, Origin of chessboard-like structures in decomposing alloys. Theoretical model and computer simulation. Acta Mater. **46**(8), 2777–2788 (1998)
24. Y. Ni, W. Rao, A.G. Khachaturyan, Pseudospinodal mode of decomposition in films and formation of chessboard-like nanostructure. Nano Lett. **9**(9), 3275–3281 (2009)
25. R.E. Newnham, D.P. Skinner, L.E. Cross, Connectivity and piezoelectric-pyroelectric composite. Mater. Res. Bull. **13**(5), 525–536 (1978)
26. R. Comes, H. Liu, M. Khokhlov, et al., Directed self-assembly of epitaxial $CoFe_2O4$-$BiFeO_3$ multiferroic nanocomposites. Nano Lett. **12**(5), 2367–2373 (2012)

27. N.M. Aimon, K.C. Hong, X.Y. Sun, et al., Templated self-assembly of functional oxide nanocomposites. Adv. Mater. **26**(19), 3063–3067 (2014)
28. G.M. Whitesides, B. Grzybowski, Self-assembly at all scales. Science **295**(5564), 2418–2421 (2002)
29. J.M. Lehn, Toward self-organization and complex matter. Science **295**(5564), 2400–2403 (2002)
30. L.G. Li, W. Zhang, F. Khatkhatay, et al., Strain and interface effects in a novel bismuth-based self-assembled supercell structure. ACS Appl. Mater. Interfaces **7**(21), 11631–11636 (2015)
31. A. Chen, Z. Bi, C.F. Tsai, et al., Tunable low-field magnetoresistance in $(La_{0.7}Sr_{0.3}MnO_3)_{0.5}$: $(ZnO)_{0.5}$, self-assembled vertically aligned nanocomposite thin films. Adv. Funct. Mater. **21** (13), 2423–2429 (2011)
32. H.K. Dong, B. Lei, N.M. Aimon, et al., Combinatorial pulsed laser deposition of Fe, Cr, Mn, and Ni-substituted $SrTiO_3$ films on Si substrates. ACS Comb. Sci. **14**(3), 179–190 (2012)
33. D.H. Kim, N.M. Aimon, C.A. Ross, Self-assembled growth and magnetic properties of a $BiFeO_3$-$MgFe_2O_4$ nanocomposite prepared by pulsed laser deposition. J. Appl. Phys. **113** (17), 17B510 (2010)
34. N.M. Aimon, H.K. Dong, K.C. Hong, et al., Deposition of epitaxial $BiFeO_3$/$CoFe_2O_4$ nanocomposites on (001) $SrTiO_3$ by combinatorial pulsed laser deposition. Appl. Phys. Lett. **100**(9), 092901–092905 (2012)
35. H.M. Christen, D.P. Norton, L.A. Géa, et al., Pulsed laser deposition of solid-solution films using segmented targets. Thin Solid Films **312**(312), 156–159 (1998)
36. A. Imai, X. Cheng, H.L. Xin, et al., Epitaxial $Bi_5Ti_3FeO_{15}$-$CoFe_2O_4$ pillar-matrix multiferroic nanostructures. ACS Nano **7**(12), 11079–11086 (2013)
37. Z. Liao, P. Gao, S. Stadler, et al., Tuning properties of columnar nanocomposite oxides. Appl. Phys. Lett. **103**(103), 043112–043116 (2013)
38. C.H. Yang, F. Yildiz, S.H. Lee, et al., Synthesis of nanoscale composites of exchange biased $MnFe_2O_4$ and Mn-doped $BiFeO_3$. Appl. Phys. Lett. **90**(16), 163116–163119 (2007)
39. H.J. Liu, L.Y. Chen, Q. He, et al., Epitaxial photostriction-magnetostriction coupled self-assembled nanostructures. ACS Nano **6**(8), 6952–6959 (2012)
40. Q. Liang, X. Bi, Nanostructure and performance of Pt–$LaNiO_3$, composite film for ferroelectric film devices. Acta Mater. **57**(14), 4109–4114 (2009)
41. J.G. Wan, X.W. Wang, Y.J. Wu, et al., Magnetoelectric $CoFe_2O_4$-Pb(Zr,Ti)O_3 composite thin films derived by a sol-gel process. Appl. Phys. Lett. **86**(12), 122501–122504 (2005)
42. X.L. Zhong, J.B. Wang, M. Liao, et al., Multiferroic nanoparticulate $Bi_{3.15}Nd_{0.85}Ti_3O_{12}$ oFe_2O_4 composite thin films prepared by a chemical solution deposition technique. Appl. Phys. Lett. **90**(15), 152903–152906 (2007)
43. H. Ryu, P. Murugavel, J. H. Lee, and S. C. Chae, Magnetoelectric coupling of multilayered $Pb(Zr_{0.52}Ti_{0.48})O_3$-$CoFe_2O_4$ film by piezoresponse force microscopy under magnetic field, Appl. Phys. Lett., vol. 89, no. 10, 102907, Jun. 2006.
44. M. Staruch, D. Hires, A. Chen, Z. Bi, Enhanced low-field magnetoresistance in $La_{0.67}Sr_{0.33}MnO_3$:MgO composite films. J. Appl. Phys. **110**(11), 3913–3918 (2011)
45. M. Staruch, C. Cantoni, M. Jain, Systematic study of magnetotransport properties and enhanced low-field magnetoresistance in thin films of $La_{0.67}Sr_{0.33}MnO_3 + Mg(O)$. Appl. Phys. Lett. **102**(6), 6436–6444 (2013)
46. S.A. Fedoseev, A.V. Pan, S. Rubanov, et al., Large, Controllable Spikes of Magnetoresistance in $La_{2/3}Ca_{1/3}MnO_3$/$SrTiO_3$ Superlattices. ACS Nano **7**(1), 286–293 (2013)
47. Y.G. Ma, W.N. Cheng, M. Ning, C.K. Ong, Magnetoelectric effect in epitaxial Pb $(Zr_{0.52}Ti_{0.48})O_3$/$La_{0.7}Sr_{0.3}MnO_3$ composite thin film. Appl. Phys. Lett. **90**(15), 15152911–15152913 (2007)
48. C. Deng, Y. Zhang, J. Ma, Y. Lin, Magnetic-electric properties of epitaxial multiferroic $NiFe_2O_4$-$BaTiO_3$, heterostructure. J. Appl. Phys. **102**(7), 7074114–7074118 (2007)
49. M. Dawber, C. Lichtensteiger, M. Cantoni, et al., Unusual behavior of the ferroelectric polarization in $PbTiO_3$/$SrTiO_3$ superlattices. Physics **95**(17), 177601–177604 (2005)

50. S.J. Callori, J. Gabel, D. Su, et al., Ferroelectric $PbTiO_3/SrRuO_3$ superlattices with broken inversion symmetry. Phys. Rev. Lett. **109**(6), 067601–067606 (2012)
51. M. Dawber, N. Stucki, C. Lichtensteiger, et al., Tailoring the properties of artificially layered ferroelectric superlattices. J. Adv. Mater. **19**(23), 4153–4159 (2007)
52. S.S.A. Seo, J.H. Lee, H.N. Lee, et al., Ferroelectricity in artificial bicolor oxide superlattices. J. Adv. Mater. **19**(18), 2460–2464 (2007)
53. K. Boldyreva, L. Pintilie, A. Lotnyk, et al., Thickness-driven antiferroelectric-to-ferroelectric phase transition of thin $PbZrO_3$ layers in epitaxial $PbZrO_3/Pb(Zr_{0.8}Ti_{0.2})O_3$ multilayers. Appl. Phys. Lett. **91**(12), 122915 (2007)
54. I. Vrejoiu, Y.L. Zhu, G.L. Rhun, et al., Structure and properties of epitaxial ferroelectric $PbZr_{0.4}Ti_{0.6}O_3/PbZr_{0.6}Ti_{0.4}O_3$ superlattices grown on $SrTiO_3$ (001) by pulsed laser deposition. Appl. Phys. Lett. **90**(7), 072909–072912 (2007)
55. R. Ramesh, N.A. Spaldin, et al., Multiferroics: progress and prospects in thin films. Nat. Mater. **6**(1), 21–29 (2007)
56. D. Tian, Q. Chen, F.Q. Nie, et al., Patterned wettability transition by photoelectric cooperative and anisotropic wetting for liquid reprography. Adv. Mater. **21**(37), 3744–3749 (2009)
57. J.L. MacManus-Driscoll, P. Zerrer, H. Wang, et al., Strain control and spontaneous phase ordering in vertical nanocomposite heteroepitaxial thin films. Nat. Mater. **7**(4), 314–320 (2008)
58. H. Yang, H. Wang, G.F. Zou, et al., Leakage mechanisms of self-assembled $(BiFeO_3)_{0.5}$: $(Sm_2O_3)_{0.5}$ nanocomposite films. Appl. Phys. Lett. **93**(14), 142904–142907 (2008)
59. X.F. Liu, J. Shi, Magnetic tunnel junctions with Al_2O_3 tunnel barriers prepared by atomic layer deposition. Appl. Phys. Lett. **102**(20), 202401–202405 (2013)
60. B. Huang, Y. Liu, R. Zhang, et al., Low-field MR behaviour in La0.67Ca0.33MnO3/ZrO2 composite system. J. Phys. D Appl. Phys. **36**(16), 1923–1927 (2003)
61. C.W. Nan, M.I. Bichurin, S. Dong, et al., Multiferroic magnetoelectric composites: historical perspective, status, and future directions. J. Appl. Phys. **103**(3), 031101–031135 (2008)
62. S. Dong, J. Zhai, J.F. Li, D. Viehland, et al., Magnetoelectric gyration effect in $Tb_{1-x}D_{yx}Fe_{2-y}$/$Pb(Zr,Ti)O_3$ laminated composites at the electromechanical resonance. Appl. Phys. Lett. **89**(24), 243512–243515 (2006)
63. Z. Wang, Y. Yang, R. Viswan, J. Li, et al., Giant electric field controlled magnetic anisotropy in epitaxial $BiFeO_3$-$CoFe_2O_4$ thin film heterostructures on single crystal $Pb(Mg_{1/3}Nb_{2/3})_{0.7}Ti_{0.3}O_3$ substrate. Appl. Phys. Lett. **99**(4), 043110–043112 (2011)
64. H.K. Dong, N.M. Aimon, Y.S. Xue, et al., Integration of self-assembled epitaxial $BiFeO_3$-$CoFe_2O_4$, multiferroic nanocomposites on silicon substrates. Adv. Funct. Mater. **24**(37), 5889–5896 (2014)
65. I. Levin, J. Li, J. Slutsker, et al., Design of self-assembled multiferroic nanostructures in epitaxial films. Adv. Mater. **18**(15), 2044–2047 (2006)
66. H. Zheng, Q. Zhan, F. Zavaliche, et al., Controlling self-assembled perovskite-spinel nanostructures. Adv. Mater. **6**(7), 1401–1407 (2006)
67. H. Zheng, F. Straub, Q. Zhan, et al., Self-assembled growth of $BiFeO_3$-$CoFe_2O_4$ nanostructures. Adv. Mater. **18**(20), 2747–2752 (2006)
68. Q. Zhan, R. Yu, S.P. Crane, et al., Structure and interface chemistry of perovskite-spinel nanocomposite thin films. Appl. Phys. Lett. **89**(17), 172902–172904 (2006)
69. N. Dix, R. Muralidharan, J.M. Rebled, et al., Selectable spontaneous polarization direction and magnetic anisotropy in $BiFeO_3$-$CoFe_2O_4$ epitaxial nanostructures. ACS Nano **4**(8), 4955–4961 (2010)
70. N. Dix, R. Muralidharan, J. Guyonnet, et al., On the strain coupling across vertical interfaces of switchable $BiFeO_3$-$CoFe_2O_4$ multiferroic nanostructures. Appl. Phys. Lett. **95**(95), 062907–062910 (2009)
71. L. Yan, Z.P. Xing, Z.G. Wang, T. Wang, et al., Direct measurement of magnetoelectric exchange in self-assembled epitaxial $BiFeO_3$-$CoFe_2O_4$ nanocomposite thin films. Appl. Phys. Lett. **94**(19), 192902 (2009)

72. Z.G. Wang, Y.X. Li, R. Viswan, B.L. Hu, et al., Engineered magnetic shape anisotropy in $BiFeO_3$-$CoFe_2O_4$ self-assembled thin films. ACS Nano **7**(4), 3447–3456 (2013)
73. S.J. Zhu, J. Yuan, B.Y. Zhu, et al., Exchange bias effect and enhanced magnetoresistance in $La_{0.67}Sr_{0.33}MnO_3$/$SrTiO_3$ superlattices. Appl. Phys. Lett. **90**(11), 112502–112505 (2007)
74. Y.-M. Kang, H.-J. Kim, S.-I. Yoo, Excellent low field magnetoresistance properties of the $La_{0.7}Sr_{0.3}Mn_{1+d}O_3$-manganese oxide composites. Appl. Phys. Lett. **95**(5), 052510–052513 (2009)
75. S. Ornes, Giant magnetoresistance, Proceedings of the National Academy of Sciences, vol. 110, no.10, pp. 3710, 2013
76. B.B. Nelsoncheeseman, F.J. Wong, R.V. Chopdekar, et al., Room temperature magnetic barrier layers in magnetic tunnel junctions. Phys. Rev. B **81**(21), 214421–214428 (2010)
77. P. P. Deen, F. Yokaichiya, A. de Santis, et al., Ferromagnetic clusters and superconducting order in $La_{0.7}Ca_{0.3}MnO_3$/$YBa_2Cu_3O_{7-\delta}$ heterostructures, Phys. Rev. B, vol. 74, no. 22, pp. 224414, 2006
78. P.P. Deen, F. Yokaichiya, A. de Santis, F. Bobba, Spin-polarized intergrain tunneling in $La_{2/3}Sr_{1/3}MnO_3$. Phys. Rev. Lett. **77**(10), 2041–2044 (1996)
79. H. Li, J.R. Sun, H.K. Wong, Enhanced low-field magnetoresistance in $La_{2/3}Ca_{1/3}MnO_3$/$Pr_{2/3}Ca_{1/3}MnO_3$ superlattices. Appl. Phys. Lett. **80**(4), 628–630 (2002)
80. S. Jin, T.H. Tiefel, M. Mccormack, et al., Thousandfold change in resistivity in magnetoresistive la-ca-mn-o films. Science **264**(5157), 413 (1994)
81. M. H. Jo, N. D. Mathur, J. E. Evetts, et al., Magnetotransport and interface magnetism in manganite heterostructures: implications for spin polarized tunneling, MRS Proceedings. Cambridge University Press, vol. 602, pp. 3, 1999
82. V. Moshnyaga, B. Damaschke, O. Shapoval, et al., Corrigendum: structural phase transition at the percolation threshold in epitaxial $(La_{0.7}Ca_{0.3}MnO_3)_{1-x}$:$(MgO)_x$ nanocomposite films. Nat. Mater. **2**(4), 247–252 (2003)
83. D. Bhadra, M.G. Masud, S.K. De, et al., Observation of large magnetodielectric and direct magnetoelectric behavior in LCMO/PVDF 0-3 nanocomposites. Appl. Phys. Lett. **102**(7), 072902–072907 (2013)
84. Y.K. Tang, X.F. Ge, X.F. Si, et al., Influence of magnetic correlations on low-field magnetoresistance in $La_{2/3}Sr_{1/3}MnO_3$/$SrTiO_3$ composites. Phys. Status Solidi A **210**(6), 1195 (2013)
85. L. Li, X. Zhang, L. Li, et al., Magnetoresistance of single-crystalline $La_{0.67}Sr_{0.33}MnO_3$/MgO nanorod arrays. Solid State Commun. **171**(10), 46 (2013)
86. J. Li, Q. Huang, Z.W. Li, et al., Enhanced magnetoresistance in Ag-doped granular $La_{2/3}Sr_{1/3}MnO_3$ thin films prepared by dual-beam pulsed-laser deposition. J. Appl. Phys. Lett. **89**(11), 7428–7430 (2001)
87. M. Staruch, H. Gao, P. Gao, et al., Low-field magnetoresistance in $La_{0.67}Sr_{0.33}MnO_3$:ZnO composite film. Adv. Funct. Mater. **22**(17), 3591 (2012)
88. L. Yan, L.B. Kong, T. Yang, et al., Magnetoresistance and current-voltage characteristics in $La_{2/3}Sr_{1/3}MnO_3$/ZnO composites. J. Appl. Phys. **96**(3), 1568–1571 (2004)
89. S.A. Köster, V. Moshnyaga, K. Samwer, et al., Doping of interfaces in $(La_{0.7}Sr_{0.3}MnO_3)_{1-x}$:$(MgO)_x$ composite films. Appl. Phys. Lett. **81**(9), 1648–1650 (2002)
90. Z. Zhang, R. Ranjith, B.T. Xie, et al., Enhanced low field magnetoresistance in nanocrystalline $La_{0.7}Sr_{0.3}MnO_3$ synthesized on MgO nanowires. Appl. Phys. Lett. **96**(22), 222501 (2010)
91. P. Kameli, H. Salamati, M. Eshraghi, et al., The effect of TiO_2 doping on the structure and magnetic and magnetotransport properties of $La_{0.75}Sr_{0.25}MnO_3$ composite. J. Appl. Phys. **98**(4), 043908–043912 (2005)
92. A. Gaur, G.D. Varma, H.K. Singh, Enhanced low field magnetoresistance in $La_{0.7}Sr_{0.3}MnO_3$/TiO_2 composite. J. Phys. D Appl. Phys. **39**(16), 3531–3535 (2006)
93. A. Gaur, G.D. Varma, Electrical and magnetotransport properties of $La_{0.7}Sr_{0.3}MnO_3$/TiO_2 composites. Cryst. Res. Technol. **42**(2), 164–168 (2007)

94. S. Valencia, O. Castaño, J. Fontcuberta, et al., Enhanced low field magnetoresistive response in $(La_{2/3}Sr_{1/3}MnO_3)_x/(CeO_2)_{1-x}$ composite thick films prepared by screen printing. J. Appl. Phys. **94**(4), 2524–2528 (2003)
95. W.J. Lu, Y.P. Sun, X.B. Zhu, et al., Low-field magnetoresistance in $La_{0.8}Sr_{0.2}MnO_3/ZrO_2$ composite system. Mater. Lett. **60**(27), 3207–3211 (2006)
96. K. Dörr, T. Walter, M. Sahana, et al., Magnetotransport of $La_{0.7}Sr_{0.3}MnO_3/SrTiO_3$ multilayers with ultrathin manganite layers. J. Appl. Phys. **89**(11), 6973–6975 (2001)
97. Z. Zi, Y. Fu, Q. Liu, et al., Enhanced low-field magnetoresistance in LSMO/SFO composite system. J. Magn. Magn. Mater. **324**(6), 1117–1121 (2012)
98. S. Gupta, R. Ranjit, C. Mitra, et al., Enhanced room-temperature magnetoresistance in $La_{0.7}Sr_{0.3}MnO_3$-glass composites. Appl. Phys. Lett. **78**(3), 362–364 (2001)
99. R.N. Mahato, H. Lülf, M.H. Siekman, et al., Ultrahigh magnetoresistance at room temperature in molecular wires. Science **341**(6143), 257–260 (2013)
100. P. Dey, T. K. Nath, Effect of grain size modulation on the magneto-and electronic-transport properties of $La_{0.7}Ca_{0.3}MnO_3$ nanoparticles: the role of spin-polarized tunneling at the enhanced grain surface, Phys. Rev. B, vol. 73, no. 21, pp. 214425, Jun. 2006.
101. A. Sadhu, S. Bhattacharyya, Enhanced low-field magnetoresistance in $La_{0.71}Sr_{0.29}MnO_3$ nanoparticles synthesized by the nonaqueous Sol-Gel route. Chem. Mater. **26**(4), 1702–1710 (2014)
102. T.H. Kim, M. Uehara, S.W. Cheong, et al., Large room-temperature intergrain magnetoresistance in double perovskite $SrFe_{1-x}(Mo\ or\ Re)_xO_3$. Appl. Phys. Lett. **74**(12), 1737–1739 (1999)
103. H.J. Liu, V.T. Tra, Y.J. Chen, et al., Large magnetoresistance in magnetically coupled $SrRuO_3$–$CoFe_2O_4$ self-assembled nanostructures. Adv. Mater. **25**(34), 4753–4759 (2013)
104. W. Zhang, A. Chen, F. Khatkhatay, et al., Integration of self-assembled vertically aligned nanocomposite $(La_{0.7}Sr_{0.3}MnO_3)_{1-x}$:$(ZnO)_x$ thin films on silicon substrates. ACS Appl. Mater. Interfaces **5**(10), 3995–3999 (2013)
105. A.P. Chen, W. Zhang, J. Jian, et al., Role of boundaries on low-field magnetotransport properties of $La_{0.7}Sr_{0.3}MnO_3$-based nanocomposite thin films. J. Mater. Res. **28**(13), 1707–1714 (2013)
106. Z. Sheng, Y. Sun, X. Zhu, et al., Enhanced low-field magnetization and magnetoresistance in nano-MgO added $La_{2/3}Ca_{1/3}MnO_3$ composites. J. Phys. D Appl. Phys. **40**(11), 3300–3305 (2007)
107. L. Joshi, S. Keshri, Extrinsic behavior in $La_{0.67}Ca_{0.33}MnO_3$-$BaTiO_3$ composites. Ceram. Int. **38**(7), 5889–5896 (2012)
108. L. Fei, L. Zhu, X. Cheng, et al., Structure and magnetotransport properties of epitaxial nanocomposite $La_{0.67}Ca_{0.33}MnO_3$: $SrTiO_3$ thin films grown by a chemical solution approach. Appl. Phys. Lett. **100**(8), 082403–082408 (2012)
109. P.K. Siwach, P. Srivastava, J. Singh, et al., Broad temperature range low field magnetoresistance in $La_{0.7}Ca_{0.3}MnO_3$: nano-ZnO composites. J. Alloys Compd. **481**(1), 17–21 (2009)
110. D.K. Satapathy, M.A. Uribe-Laverde, I. Marozau, et al., Magnetic Proximity Effect in $YBa_2Cu_3O_7/La_{2/3}Ca_{1/3}MnO_3$ and $YBa_2Cu_3O_7/LaMnO_{3+\sigma}$Superlattices. Phys. Rev. Lett. **108**(19), 197201–197206 (2012)
111. A.V. Ustinov, V.K. Kaplunenko, Rapid single-flux quantum logic using π-shifters. J. Appl. Phys. **94**(8), 5405–5407 (2003)
112. A.I. Buzdin, Proximity effects in superconductor-ferromagnet heterostructures. Rev. Mod. Phys. **77**(3), 935–976 (2005)
113. M.J.M. De Jong, C.W.J. Beenakker, Andreev reflection in ferromagnet-superconductor junctions. Phys. Rev. Lett. **74**(9), 1657–1660 (1995)
114. R.J. Soulen, J.M. Byers, M.S. Osofsky, et al., Measuring the spin polarization of a metal with a superconducting point contact. Science **282**(5386), 85–88 (1998)
115. S. K. Upadhyay, A. Palanisami, R. N. Louie, et al., Probing ferromagnets with Andreev reflection, Phys. Rev. Lett., vol. 81, no. 15, pp. 3247, Oct. 1998.

116. Z. Y. Chen, A. Biswas, I. Žutić, et al, Spin-polarized transport across a $La_{0.7}Sr_{0.3}MnO_3$/$YBa_2Cu_3O_{7-x}$ interface: role of Andreev bound states, Phys. Rev. B, vol. 63, no. 21, pp. 212508, May 2001.
117. T. Holden, H.U. Habermeier, G. Cristiani, et al., Proximity induced metal-insulator transition in $YBa_2Cu_3O_7/La_{2/3}Ca_{1/3}MnO_3$ superlattices. Phys. Rev. B **69**(6), 064505–064512 (2004)
118. A. Hoffmann, S.G.E. Te Velthuis, Z. Sefrioui, et al., Suppressed magnetization in $La_{0.7}Ca_{0.3}MnO_3/YBa_2Cu_3O_{7-\delta}$ superlattices. Phys. Rev. B **72**(14), 140407–140411 (2005)
119. J. Chakhalian, J.W. Freeland, G. Srajer, et al., Magnetism at the interface between ferromagnetic and superconducting oxides. Nat. Phys. **2**(4), 244–248 (2006)
120. A.F. Volkov, K.B. Efetov, Proximity effect and its enhancement by ferromagnetism in high-temperature superconductor-ferromagnet structures. Phys. Rev. Lett. **102**(7), 077002–077006 (2009)
121. R. Werner, C. Raisch, A. Ruosi, et al., $YBa_2Cu_3O_7/La_{0.7}Ca_{0.3}MnO_3$ bilayers: interface coupling and electric transport properties. Phys. Rev. B **82**(22), 224509–224516 (2010)
122. J. Chakhalian, J.W. Freeland, H.-U. Habermeier, et al., Orbital reconstruction and covalent bonding at an oxide interface. Science **318**(5853), 1114–1117 (2007)
123. G. M. De Luca, G, Ghiringhelli, C. A. Perroni, et al., "Ubiquitous long-range antiferromagnetic coupling across the interface between superconducting and ferromagnetic oxides," Nat. Commun., vol. 5, no. 6, pp. 5626-5633, 2014.
124. L.F. Kourkoutis, J. Chakhalian, B. Gray, et al., Visualizing short-range charge transfer at the interfaces between ferromagnetic and superconducting oxides. Nat. Commun. **4**(4), 2336–2343 (2013)
125. J.L. MacManus-Driscoll, S.R. Foltyn, Q.X. Jia, et al., Strongly enhanced current densities in superconducting coated conductors of $YBa_2Cu_3O_{7-x}$+ $BaZrO_3$. Nat. Mater. **3**(7), 439–443 (2004)
126. S. Kang, A. Goyal, J. Li, et al., High-performance high-T*c* superconducting wires. Science **311**(5769), 1911–1914 (2006)
127. J. Gutiérrez, A. Llordes, J. Gazquez, et al., Strong isotropic flux pinning in solution-derived $YBa_2Cu_3O_{7-x}$ nanocomposite superconductor films. Nat. Mater. **6**(5), 367–373 (2007)
128. B. Maiorov, S. A. Baily, H, Zhou, et al., "Synergetic combination of different types of defect to optimize pinning landscape using $BaZrO_3$-doped $YBa_2Cu_3O_7$," Nat. Mater., vol. 8, no. 5, pp. 398-404, 2009.
129. C. Cantoni, Y. Gao, S.H. Wee, et al., Strain-driven oxygen deficiency in self-assembled, nanostructured, composite oxide films. ACS Nano **5**(6), 4783–4789 (2011)
130. S.H. Wee, Y. Gao, Y.L. Zuev, et al., Self-assembly of nanostructured, complex, multication films via spontaneous phase separation and strain-driven ordering. Adv. Funct. Mater. **23**(15), 1912–1918 (2013)
131. M. Dawber, E. Bousquet, New developments in artificially layered ferroelectric oxide superlattices. MRS Bull. **38**(12), 1048–1055 (2013)
132. H.N. Lee, H.M. Christen, M.F. Chisholm, et al., Strong polarization enhancement in asymmetric three-component ferroelectric superlattices. Nature **433**(7024), 395–399 (2005)
133. E. Bousquet, M. Dawber, N. Stucki, et al., Improper ferroelectricity in perovskite oxide artificial superlattices. Nature **452**(7188), 732–736 (2008)
134. C.H. Ahn, K.M. Rabe, J.M. Triscone, Ferroelectricity at the nanoscale: local polarization in oxide thin films and heterostructures. Science **303**(5657), 488–491 (2004)
135. P. Zubko, S. Gariglio, M. Gabay, et al., Interface physics in complex oxide heterostructures. Annu. Rev. Condens. Matter Phys. **2**(1), 141–165 (2011)
136. H. Tabata, H. Tanaka, T. Kawai, Formation of artificial $BaTiO_3/SrTiO_3$ superlattices using pulsed laser deposition and their dielectric properties. Appl. Phys. Lett. **65**(15), 1970–1972 (1994)
137. N. A. Pertsev, V. G. Kukhar, H. Kohlstedt, et al., Phase diagrams and physical properties of single-domain epitaxial $Pb(Zr_{1-x}Ti_x)O_3$ thin films, Phys. Rev. B, vol. 67, no. 5, pp. 054107, Feb. 2003.

138. J. X. Zhang, D. G. Schlom, L. Q. Chen, et al., Tuning the remanent polarization of epitaxial ferroelectric thin films with strain, Appl. Phys. Lett., vol. 95, no. 12, pp. 122904, Sep 2009.
139. C. Ederer, N. A. Spaldin, Effect of epitaxial strain on the spontaneous polarization of thin film ferroelectrics, Phys. Rev. Lett., vol. 95, no. 25, pp. 257601, Dec. 2005.
140. M. D. Nguyen, M. Dekkers, E. Houwman, et al., Misfit strain dependence of ferroelectric and piezoelectric properties of clamped (001) epitaxial $Pb(Zr_{0.52}, Ti_{0.48})O_3$ thin films, Appl. Phys. Lett., vol. 99, no. 25, pp. 252904, Dec. 2011.
141. K.J. Choi, M. Biegalski, Y.L. Li, et al., Enhancement of ferroelectricity in strained $BaTiO_3$ thin films. Science **306**(5698), 1005–1009 (2004)
142. J.H. Haeni, P. Irvin, W. Chang, et al., Room-temperature ferroelectricity in strained $SrTiO_3$. Nature **430**(7001), 758–761 (2004)
143. D. G. Schlom, L. Q. Chen, C. B. Eom, et al., Strain tuning of ferroelectric thin films, Annu. Rev. Mater. Res. vol. 37, no. 126, pp. 589-626, May. 2007.
144. F.F. Ge, L. Bai, W.D. Wu, et al., The controllable growth of Co-$BaTiO_3$ nanocomposite epitaxial film by laser molecular beam epitaxy. J. Cryst. Growth **312**(16), 2489–2493 (2015)
145. F.F. Ge, X.M. Wang, L.H. Cao, et al., Self-organized Ni nanocrystal embedded in $BaTiO_3$ epitaxial film. Nanoscale Res. Lett. **5**(5), 834–838 (2010)
146. Y.J. Wu, H.L. Wang, X.K. Ning, et al., Dielectric properties of Au-$BaTiO_3$ nanocomposite films prepared by Sol-Gel method. J. Inorg. Mater. **30**(2), 207–213 (2015)
147. O.J. Lee, S.A. Harrington, A. Kursumovic, et al., Extremely high tunability and low loss in nanoscaffold ferroelectric films. Nano Lett. **12**(8), 4311–4317 (2012)
148. B. Houng, Tin doped indium oxide transparent conducting thin films containing silver nanoparticles by sol-gel technique. Appl. Phys. Lett. **87**, 251922 (2005)
149. H.L. Wang, Y. Bai, X.K. Ning, Z.J. Wang, Enhanced electrical properties in ferroelectric thin films on conductive Au-$LaNiO_3$ nanocomposite electrodes via modulation of Schottky potential barrier. RSC Adv. **5**(126), 104203–104209 (2015)